NANO LETTERS

LETTER

pubs.acs.org/NanoLett

Inducing Electronic Changes in Graphene through Silicon (100) Substrate Modification

Y. Xu,[*,†,‡,∥] K. T. He,[‡,∥] S. W. Schmucker,[‡] Z. Guo,[†] J. C. Koepke,[‡] J. D. Wood,[‡] J. W. Lyding,[*,‡] and N. R. Aluru[§]

[†]Department of Information Science and Electronic Engineering, Zhejiang University, Hangzhou 310027, People's Republic of China

[‡]Department of Electrical and Computer Engineering, Beckman Institute for Advanced Science and Technology, University of Illinois, Urbana, Illinois 61801, United States

[§]Department of Mechanical Science and Engineering, Beckman Institute for Advanced Science and Technology, University of Illinois at Urbana−Champaign, Urbana, Illinois 61801, United States

Supporting Information

ABSTRACT: We have performed scanning tunneling microscopy and spectroscopy (STM/STS) measurements as well as *ab initio* calculations for graphene monolayers on clean and hydrogen(H)-passivated silicon (100) (Si(100)/H) surfaces. In order to experimentally study the same graphene piece on both substrates, we develop a method to depassivate hydrogen from under graphene monolayers on the Si(100)/H surface. Our work represents the first demonstration of successful and reproducible depassivation of hydrogen from beneath monolayer graphene flakes on Si(100)/H by electron-stimulated desorption. *Ab initio* simulations combined with STS taken before and after hydrogen desorption demonstrate that graphene interacts differently with the clean and H-passivated Si(100) surfaces. The Si(100)/H surface does not perturb the electronic properties of graphene, whereas the interaction between the clean Si(100) surface and graphene changes the electronic states of graphene significantly. This effect results from the covalent bonding between C and surface Si atoms, modifying the π-orbital network of the graphene layer. The local density of states shows that the bonded C and Si surface states are highly disturbed near the Fermi energy.

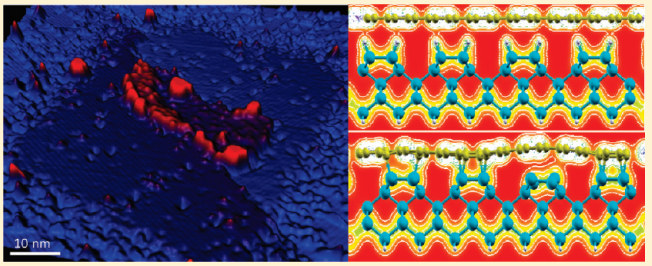

KEYWORDS: Graphene, Silicon, scanning tunneling microscopy, electron-stimulated desorption, DFT

Graphene has many unusual electronic properties, including high carrier mobility and long mean free path,[1−9] making it a promising candidate for next-generation nanoelectronic devices. Practical monolayer graphene devices require a supporting substrate, muting many of graphene's astonishing electronic properties through substrate-induced perturbations. Understanding the electronic and topographic properties of graphene as well as its interaction with a supporting substrate is critical to successfully integrate graphene into future nanoelectronic devices. Previous experimental studies and theoretical analysis of graphene monolayers on silicon carbide (SiC)[10−15] and SiO_2[16] show that strong graphene−substrate interactions break the graphene π-orbital network and thus degrade the electronic properties of graphene monolayers. Few theoretical calculations exploring the interaction between graphene and Si(100) have been presented[17] despite silicon's wide semiconductor industry use and extensive surface studies.[18−20]

Our goal is to study interactions between monolayer graphene and the Si(100) substrate using scanning tunneling microscopy (STM) as well as *ab initio* simulation. STM is an ideal tool for studying graphene−substrate interactions due to its ability to achieve atomic spatial resolution and to probe local electronic properties by scanning tunneling spectroscopy (STS).[21,22] We performed room temperature STM and STS on nanoscale graphene flakes deposited by dry contact transfer (DCT)[23] onto the Si(100)-2 × 1/H surface, a technique employed previously by Ritter and Lyding.[24] This technique has also been employed to study carbon nanotubes (CNTs) deposited on Si(100).[25] After identifying and characterizing monolayer graphene on the Si(100)-2 × 1/H surface, we desorbed hydrogen from both under and around the graphene using electron-stimulated desorption (ESD). We acquire STS data before and after the hydrogen desorption to measure the change in the electronic properties of graphene.

Controlled desorption of hydrogen from the Si(100)/H surface breaks hydrogen−silicon bonds by using emitted electrons from the STM tip, giving a chemically active array of silicon dangling bonds. This technique has been extensively explored on the Si(100) surface,[26,27] but our work represents the first demonstration of successful and reproducible depassivation beneath monolayer graphene flakes. We performed all measurements with a home-built ultrahigh vacuum (UHV) STM at 300 K with a base pressure below 1×10^{-10} Torr. Hydrogen-passivated silicon was prepared and DCT was performed in situ.

Received: March 28, 2011
Revised: May 18, 2011
Published: June 10, 2011

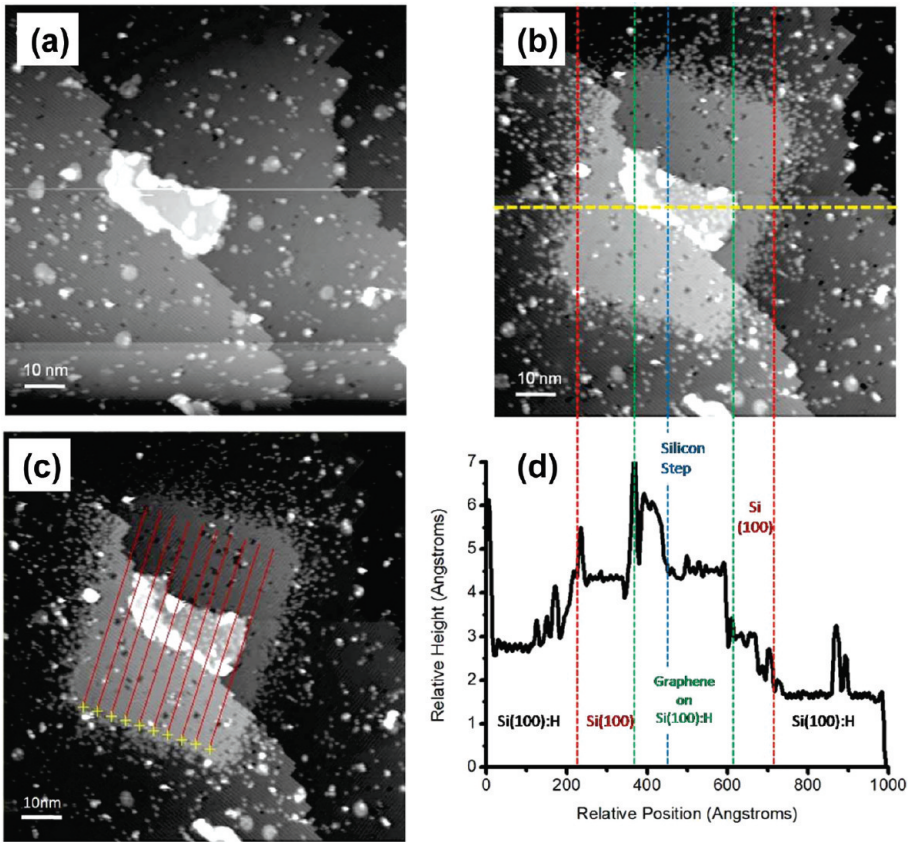

Figure 1. (a) Monolayer graphene on the Si(100)/H surface. The size of the graphene flake is approximately 12 × 30 nm with an apparent height of 3.2 Å. The difference in apparent height between Si(100)/H and clean Si(100) is ∼1.5 Å and is due to the increased density of electronic states from the silicon dangling bonds.[36] Part of the flake is draped along an atomic step edge on the silicon surface. (b) Graphene enclosed by a box of depassivated Si(100) with subgraphene dangling bonds, as indicated by protrusions visible through the graphene. (c) Path of STM tip during depassivation, where the yellow Xs indicate where the lines originated. The writing parameters for each line were +7.0 V sample bias, 2 nA current set point, and a line dose of 0.002 C/cm. The depassivated box and the dangling bonds underneath the graphene were created simultaneously using ten individual nanolithographic lines, following the solid red lines in (c). (d) Topographic contour taken of (b) indicated by the dotted yellow line. The STM images were taken at −2 V sample bias and 50 pA tunneling current.

The dI/dV and $(dI/dV)/(I/V)$ were calculated from raw tunneling current (I) versus sample bias (V) data taken during STS and Gaussian smoothed. The graph of $(dI/dV)/(I/V)$ versus sample bias provides an estimation of the graphene local density of states (LDOS), and it allows a measurement of the graphene band gap.[24] Hydrogen desorption was performed at +6 to +8 V sample bias with a 2 nA current set point. Line doses ranging from 0.02 to 0.04 C/cm were found to be most effective.

In Figure 1, a graphene flake is shown before and after hydrogen desorption, using the same parameters as hydrogen desorption on Si(100)/H (2 nA tunneling current, +7 V sample bias, 0.002 C/cm line dose). The apparent height of the graphene on Si(100)/H is 3.2 Å, similar to values reported in previous studies.[24] The bright dots that appear underneath the graphene after desorption are dangling bonds created by removal of hydrogen from the underlying silicon. However, unlike depassivation of normal Si(100)/H, the depassivation pattern under graphene appears to be spatially delocalized. It is possible to obtain almost complete depassivation underneath a small graphene flake, as shown in later figures, but the process requires a higher sample bias and a larger electron dose than that normally required for ESD of hydrogen from silicon. We suspect that the tunneling electrons from the tip are spreading out in the graphene flake before dissipating to the substrate, which explains the delocalized nature of resulting ESD patterns, and the limitation of full depassivation to small flakes of graphene. For the cases where we do obtain nearly full hydrogen depassivation, the underlying Si(100) dimer rows become visible, as predicted in our *ab initio* STM simulations.

In Figure 2a,b, we show another graphene flake before and after hydrogen desorption. The line doses used in this case are ten times greater than that used in Figure 1, which along with the small size of the flake accounts for the higher density of dangling bonds created under the graphene. The visibility of the underlying dimers after depassivation, as demonstrated by the line contours in Figure 2c,d, appears very similar to a graphene semitransparency effect observed previously on GaAs(110), InAs(110),[28] and on SiC.[29] However, in those studies the semitransparency is due to the wave functions of the surface dangling bonds protruding through the graphene at high sample bias, as is clearly demonstrated by a bias-dependence of the semitransparency. In the case of graphene on clean Si(100), the semitransparency is bias-independent in both experimental and simulated STM images, which suggests a stronger interaction between the graphene and silicon surface.

dx.doi.org/10.1021/nl201022t |*Nano Lett.* 2011, 11, 2735–2742

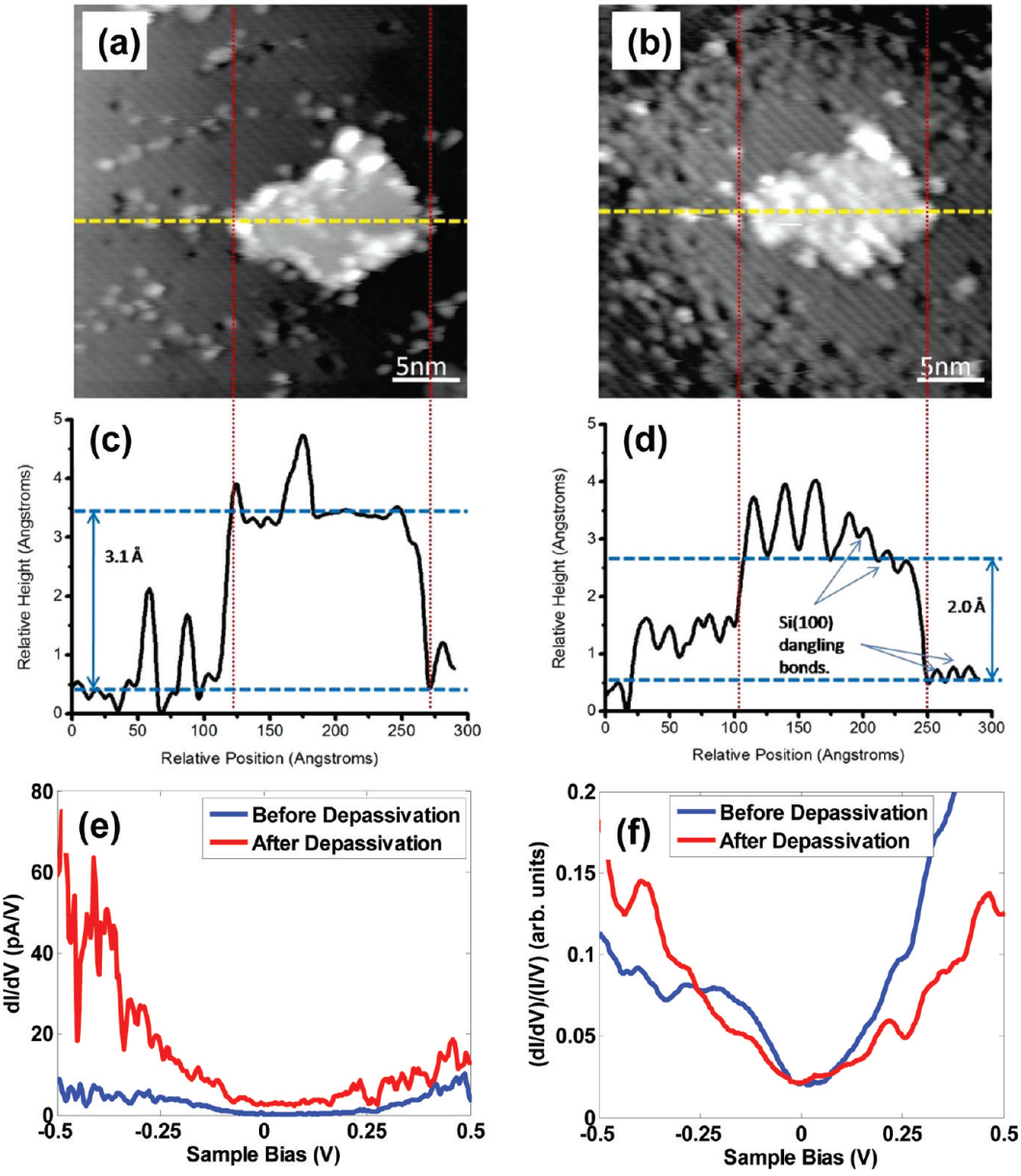

Figure 2. (a) An 8 × 12 nm metallic monolayer graphene flake on Si(100)/H with an apparent height of ~3.1 Å. Notice that the underlying Si(100) lattice is not visible through the graphene. (b) Graphene on depassivated Si(100) with the underlying surface mostly depassivated. The characteristic dimer row structure of the Si(100) 2 × 1 reconstruction is visible through the graphene flake. The apparent height of the graphene flake is 0.2 nm. (c) Topographic contour of (a) taken at the location of the dotted yellow line. Notice again that the underlying substrate contours are not visible through the graphene. (d) Topographic contour of (b) taken at the location of the dotted yellow line. The Si(100) dangling bonds are now clearly visible through the graphene flake. Graphs in (e) and (f) showing the computed dI/dV and (dI/dV)/(I/V) spectra of the graphene before and after depassivation. Each plotted line is an average of seventeen spectra points taken on the graphene. Unfortunately, the graphene lattice cannot be resolved in order to confirm the edge geometry. In (f), the band structure remains metallic after depassivation, meaning hydrogen desorption from the underlying substrate did not alter the graphene electronic structure appreciably near the Fermi level (0 V sample bias). The change in the graphene's LDOS away from the Fermi level may result from interactions with depassivated Si(100) on the graphene periphery. The STM images of (a) and (b) were taken at −2 V sample bias and 50 pA tunneling current.

STS taken before and after hydrogen desorption under the graphene offers some insight into how graphene interacts with the clean Si(100) and the Si(100)/H surface. Figure 2e,f shows the dI/dV and (dI/dV)/(I/V) plots (computed from experimentally obtained I−V data) of a metallic graphene flake before and after hydrogen desorption. The absence of a size-effect energy gap in this flake is most likely due to metallic zigzag edge states.[24] While there is no increase in the size of the graphene energy gap due to hydrogen depassivation, there is a noticeable upward shift in the graphene dI/dV, which is also confirmed in our simulated dI/dV curves obtained from *ab initio* transport simulation.

Figure 3a,b shows another small graphene flake before and after hydrogen desorption. As seen in Figure 3c, the small graphene flake has a clear band gap on the Si(100)/H substrate. After hydrogen desorption, the band gap disappears, and the

dx.doi.org/10.1021/nl201022t |*Nano Lett.* 2011, 11, 2735–2742

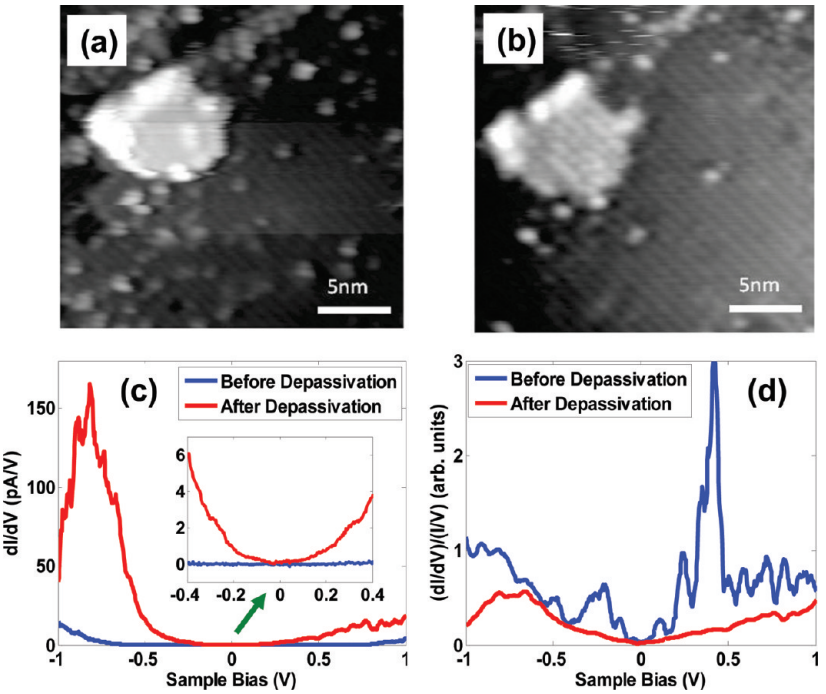

Figure 3. (a) A 7 × 9 nm monolayer graphene flake on Si(100)/H. (b) Graphene flake after almost complete hydrogen desorption from Si(100), as indicated by the visibility of the Si(100) lattice underneath the graphene. (c) Comparison of the average computed dI/dV of eleven spectra points before and after hydrogen desorption. The computed (dI/dV)/(I/V) is shown in (d). From the dI/dV, one can see a clear reduction in the apparent graphene band gap. Something similar can be seen in the computed (dI/dV)/(I/V), where it appears the graphene transitions from a semiconducting state to a metallic state, matching the plots of figure 2e. The large peak seen in the computed (dI/dV)/(I/V) can be attributed to edge states in the graphene. The STM topographs of (a) and (b) were taken at −2 V sample bias and 50 pA tunneling current.

graphene appears metallic as seen in Figure 3d. Looking at the computed dI/dV curves in Figure 3c and the computed dI/dV/(I/V) curves in Figure 3d, we observe a significant change in the graphene band gap after the surface is modified. The graphene piece went from having a sizable quantum confinement band gap to being essentially metallic. Our theoretical studies indicate that the disappearance of the graphene band gap results from the enhanced electronic interactions between graphene and clean Si(100), as compared to the interaction between graphene and Si(100)/H. This result also implies an adsorption energy reduction for graphene flakes on the H-passivated Si surface in comparison with that for graphene flakes on the clean Si surface. We verify this result with our simulation work in the following discussion.

In order to better understand our experimental results, we applied density functional theory (DFT) to simulate graphene flakes and graphene sheets with H-passivated edges on Si(100) surfaces using the local density approximation (LDA)[30] in the SIESTA code.[31] The equilibrium coordinates of the hybrid structures after full relaxation are shown in Figure 4, which are determined by the balance of the bonding and the elastic energy with maximum residual forces less than 0.01 eV/ Å. The simulated STM images at applied sample biases were approximated by a simple integral of the surface local density of states at the tip position. The simulated tunneling currents are computed by varying applied biases between the graphene covered Si substrates and the tungsten tip with three layers of atoms at a distance of 0.2 nm.

For the initial nanoscale graphene flake on Si(100)-2 × 1/H substrate system shown in Figure 4a, the corresponding charge density isosurfaces shown in Figure 4e clearly indicate an absence of covalent bonding between C and Si atoms. Since the Si dangling bonds are passivated by H atoms, the dominant interaction between C and Si atoms is by van der Waals forces. The large spacing between the graphene and the H-passivated Si substrate is due to the difficulty of DFT to describe the van der Waals force accurately.[32] As hydrogen passivation renders the surface chemically inert, the electronic states of the combined Si(100)2 × 1/H and graphene flake system remain with no apparent modification. This result is consistent with previous experimental work[24,25] and is again confirmed in this work, shown by Figure 3a,c. The typical LDOS from the nearest neighboring Si and C pair before depassivation, shown in Figure 5, clearly indicates that surface Si and C atoms do not interact with each other, as energy states from Si and C have no common energy levels within the energy gap. A similar effect occurs for CNTs on H-passivated Si(100).[33]

For the graphene flake on Si(100) after hydrogen desorption as seen in Figure 4b, the corresponding charge density contours are shown in Figure 4f. The surface Si bonding atoms relax outward, whereas the partner graphene atoms move toward the substrate. The carbon atoms are adsorbed on the surface, reacting with the high density of dangling bonds on the clean silicon surface. In the relaxed stable geometry shown in Figure 4b, Si−C chemical covalent bonds are formed. The Si−C bond lengths range from 1.93 to 2.05 Å. The Si−C bonds are close to the SiC bond length (1.92 Å), indicating that the bonding strength of Si−C surface bonds is similar to that of crystalline SiC bonds. The change in graphene height from ∼3 Å (Figure 2c) on Si(100)/H to ∼2 Å on clean Si(100) (Figure 2d) obtained from STM also matches well with the simulation. The reason for the

dx.doi.org/10.1021/nl201022t |*Nano Lett.* 2011, 11, 2735–2742

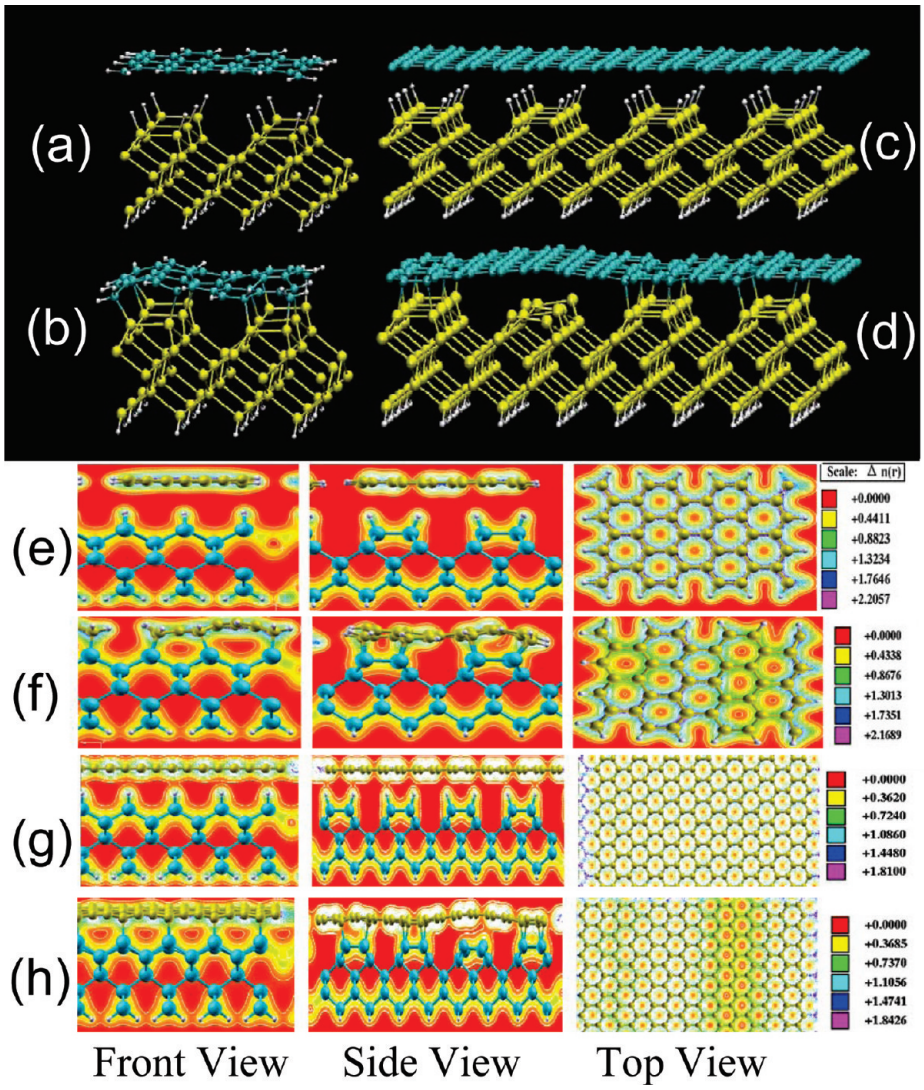

Figure 4. Geometries and charge density contour plots (spacing in electrons per Å^3) of the graphene adsorbed on silicon surfaces. The structures are fully relaxed with residual forces less than 0.01 eV/Å. (a) A graphene flake with 3 × 3 unit cells adsorbed on the Si(100)-2 × 1/H surface. (b) A graphene flake with 3 × 3 unit cells adsorbed on the clean Si(100)-2 × 1 surface. (c) An infinite graphene sheet adsorbed on the Si(100)-2 × 1/H surface. (d) An infinite graphene sheet adsorbed on the clean Si(100)-2 × 1 surface. Their corresponding charge density contour plots are shown in (e−h) to visualize the interaction between the graphene monolayer and the Si substrate. After full geometry optimization and relaxation, no covalent bonding between C and Si atoms is found near the Si (100)-2 × 1/H surface. For the clean Si(100)-2 × 1 surface case, the graphene sheets are attached to the dangling Si surface atoms, and surface−graphene Si−C σ-bonds are formed.

striking difference between the two graphene-covered surfaces becomes clear when we compare the density isosurface localization of the two structures. As seen in Figure 4f for the clean Si surface, the interface electron density is strongly delocalized. The energy gap of the graphene flake on the clean Si(100) surface is much smaller than that on the Si(100)-H surface as shown in Figure 5a,b. Figure 3e experimentally corroborates this result. The typical partial LDOS of the nearest neighboring Si and C pair after hydrogen desorption in Figure 5 show that the surface Si and C states have common energy levels near the Fermi energy. The energy states associated with Si−C bonds increase the density of states near the Fermi level, and therefore electron clouds are overlapped throughout the graphene−surface contact, as also shown in STM dI/dV curves of Figure 2e and Figure 3d. Therefore, electrons within the common energy levels can travel between the bonded graphene and Si surface atoms, indicating a strong interaction between the bonded graphene and Si surface atoms.

For the infinite graphene sheets shown in Figure 4c,d, the corresponding charge density contours are shown in Figure 4g,h. The simulated STM images in Figure 6a and the experimental STM images in Figure 2a and Figure 3a also show that the electron states of graphene structures retain their delocalized character for the H-passivated surface. In contrast, for infinite graphene sheets given in Figure 4d, there is charge localization at the positions of Si−C bonds in Figure 4h. The formation of Si−C bonds is highly dependent on the interface atomic geometries. Previous density-functional theory calculations[34] found metallic single-wall CNTs on clean Si(100) surfaces form covalent bonds to Si(100). Because of CNT curvature, the CNT−Si(100) interaction is reduced to the carbon atoms in the circumference that are in closer contact to Si(100). As discussed here, graphene

dx.doi.org/10.1021/nl201022t |*Nano Lett.* 2011, 11, 2735–2742

flakes and full-coverage graphene do form covalent bonds to clean Si(100) surfaces similar to metallic nanotubes.[35] We also notice that similar simulation work has been done in ref 17. They simulated zigzag GNRs on clean Si(100) surfaces and observed ribbon edge C atoms are bonded with Si surface atoms. In our instance, we found that not only edge C atoms, but also inner C atoms of graphene monolayers formed Si−C bonds with Si surface atoms. The difference may come from the high sensitivity of graphene width and direction dependent interface hybridization.[17] We also computed the structural and electronic properties of graphene GNRs on clean and H-passivated Si(100) in the supporting material section, which provides a comprehensive analysis of the depassivation process of H atoms from beneath monolayer graphene on Si(100)/H by ESD.

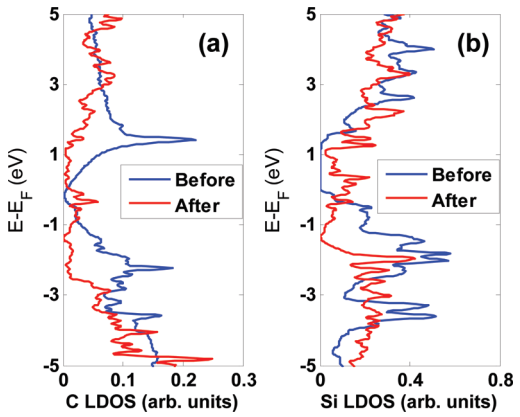

Figure 5. (a) LDOS of the C atom in a typical nearest neighboring C−Si atom pair before and after hydrogen depassivation of the graphene-covered Si structure in Figure 4a,b. (b) LDOS of the Si atom in a typical nearest neighboring C−Si atom pair before and after hydrogen depassivation. Blue and red curves are the LDOS before and after hydrogen depassivation, respectively. The energy states associated with Si−C bonds increase the density of states near the Fermi level, and therefore electron clouds are overlapped throughout the graphene−surface contact, as also shown in STM dI/dV curves of Figure 2e and 3d.

Our simulated tunneling current between the STM tungsten tip and the graphene-covered Si substrates, shown in Figure 7, also shows similar enhancement of vertical transport conductivity after depassivation, further supporting strong graphene−substrate interaction and matching the experimental plots of Figure 2e and Figure 3c,d. In the case of graphene on Si(100) after hydrogen desorption, transparency of Si dimer rows beneath the graphene sheet exists under various biases in simulated STM images (Figure 6b) as well as experimental STM images (Figure 6c). Our calculations confirm experimental evidence for strong bonding between graphene and the clean Si surface by the bias-insensitive visibility of silicon dimer rows through graphene after depassivation as well as by the visibility of the Si(111) surface through graphene monolayers.[36] Si−C chemical bonds are also found at the graphene−Si(100) interface as shown in Figure 4f,h. The Si−C bond lengths range from 1.97 to 2.06 Å. The covalent bonding drastically changes the graphene DOS near the Fermi energy. The Mulliken charges on the Si atoms of the Si−C bonds range from 0.21 to 0.25 e, whereas the Mulliken charges on C atoms of the Si−C bonds range from −0.11 to −0.14 e. Surface state electrons transfer from the Si surface to the graphene monolayer, and thus the graphene becomes n-doped and negatively charged. These findings are consistent with the SiC chemical structures, where the Si atoms are positively charged

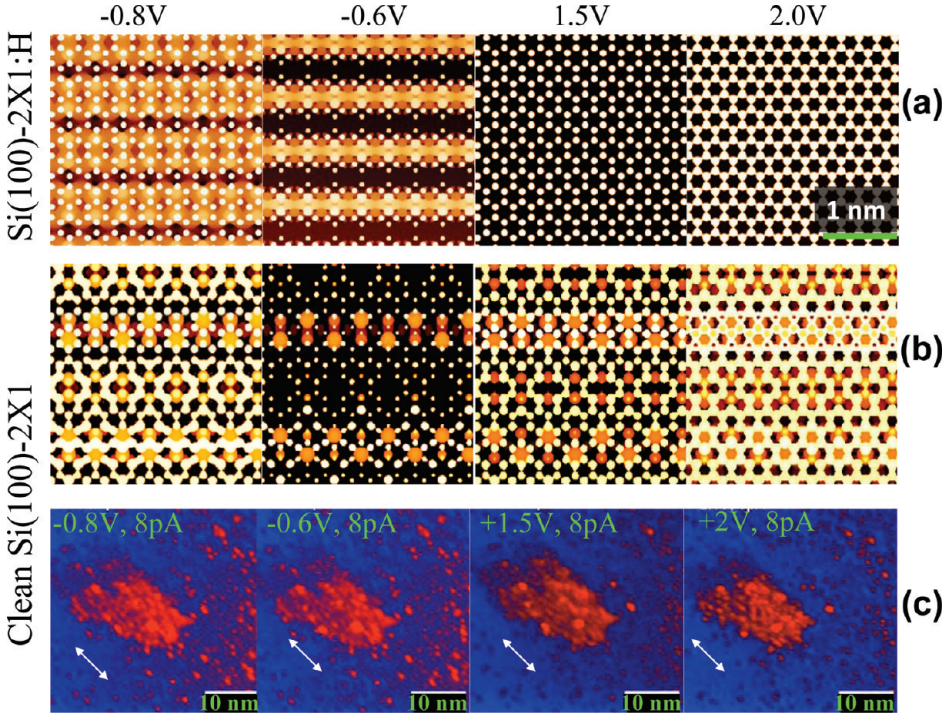

Figure 6. Comparison between the simulated STM images before and after hydrogen depassivation of the graphene-covered Si structure in Figure 4c,d. For the Si(100)/H case shown in (a), the substrate is visible through the graphene only at low bias, which is consistent with our previous work in ref 24. The silicon dimer rows are visible through the graphene at all biases after hydrogen depassivation as shown in (b), indicating the electron states of silicon are highly mixed with those of graphene. This is consistent with our experimental STM measurements shown in (c). The arrows show the Si(100) dimer row directions.

dx.doi.org/10.1021/nl201022t |*Nano Lett.* 2011, 11, 2735–2742

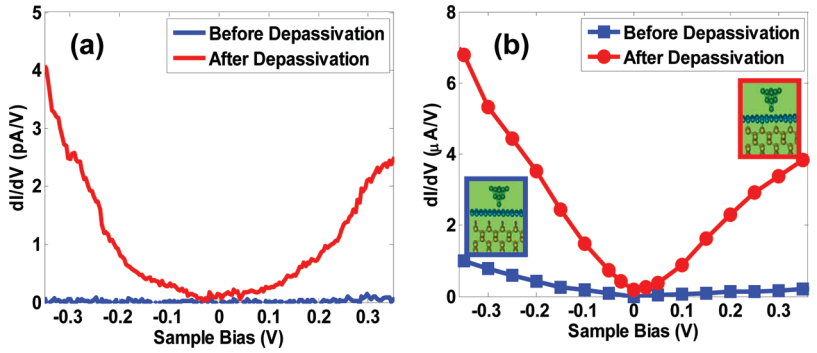

Figure 7. The experimental (a) and simulated (b) tunneling dI/dV versus V curves are compared. The experimental STM curves are a zoomed-in version of Figure 3c. The simulated STM curves are obtained by computing the tunneling currents between the graphene−Si substrate and the tungsten tip with three layers of atoms. The bottom-most atom of the STM tip is located exactly 0.2 nm above the plane of graphene hexagonal ring. The simulated tunneling dI/dV versus V curves are an average of seven different sampling tip positions, where six of them located on the each corner of a graphene hexagonal ring, and the seventh located on the center of the hexagonal ring. There is a noticeable upward shift in the dI/dV of the graphene after depassivation in (a), suggesting that it took on a more metallic character, which is also observed in our simulated dI/dV curves shown in (b).

and C atoms are negatively charged. Thus, a PN junction might be formed between the p-doped Si substrate and the charge-transfer induced n-type graphene, which may find application in rectification and diodes.

In summary, STM and STS experiments are used to investigate the electronic properties of nanometer-scale graphene deposited onto H-passivated and clean Si(100) substrates, which are confirmed using *ab initio* DFT calculations. Our experimental results of graphene on Si(100) after hydrogen desorption show a reduced graphene apparent height as well as a semitransparency effect. There is also significant modification of graphene electronic states following electron-stimulated hydrogen desorption. We can ascribe this to the LDOS modification from surface reconfiguration, electronic charge transfer from the Si substrates to the graphene monolayer, resulting in a PN junction between the p-type Si surface and charge transfer-induced n-type graphene. Our experiment highlights the importance of graphene−substrate interactions, as we are able to modify the electronic structure of a graphene flake by inducing changes in the substrate underneath. We are currently studying the depassivation and desorption mechanism of the hydrogen atoms, as this information could lead to controllable, localized modification of the hydrogen-passivated silicon underneath graphene, which would in turn allow us to fabricate novel graphene nanodevices. Finally, our results may shed some light on the mechanism by which hydrogen intercalates between graphene and SiC, leading to the production of higher quality epitaxial graphene on that substrate.[37]

■ ASSOCIATED CONTENT

Supporting Information. Additonal information. This material is available free of charge via the Internet at http://pubs.acs.org.

■ AUTHOR INFORMATION

Corresponding Author

*E-mail: (Y.X.) yangxu-isee@zju.edu.cn; (J.W.L.) lyding@illinois.edu.

Author Contributions

‖These authors (Yang Xu and K. T. He) contributed equally to this work.

■ ACKNOWLEDGMENT

The authors would like to thank Professor Yuanbo Zhang, Dr. Salvador Barraza-Lopez, and Dr. Hui Zeng for fruitful discussions. Calculations were performed on the Apple Turing Cluster at University of Illinois. This research is supported by NSF under Grant 0941497, the Office of Naval Research under Grant N00014-06-101290, the National Science Foundation of China under Grant 61006077, and the Natural Basic Research Program of China under Grant 2007CB613405. Y.X. is also supported by the Excellent Young Faculty Awards Program (Zijin Plan) at Zhejiang University and Specialized Research Fund for the Doctoral Program of Higher Education (SRFDP with Grant 20100101120045).

■ REFERENCES

(1) (a) Novoselov, K. S.; Geim, A. K.; Morozov, S. V.; Jiang, D.; Katsnelson, M. I.; Grigorieva, I. V.; Dubonos, S. V.; Firsov, A. A. *Nature* **2005**, *438*, 197. (b) Zhang, Y.; Tan, Y.-W.; Stormer, H. L.; Kim, P. *Nature* **2005**, *438*, 201. (c) Berger, C.; Song, Z.; Li, X.; Wu, X.; Brown, N.; Naud, C.; Mayou, D.; Li, T.; Hass, J.; Marchenkov, A. N.; Conrad, E. H.; First, P. N.; de Heer, W. A. *Science* **2006**, *312*, 1191–1196. (d) Neto, A. H. C.; Guinea, F.; Peres, N. M. R.; Novoselov, K. S.; Geim, A. K. *Rev. Mod. Phys.* **2009**, *81*, 109.

(2) Han, M. Y.; Ozyilmaz, B.; Zhang, Y.; Kim, P. *Phys. Rev. Lett.* **2007**, *98*, 206805.

(3) Chen, Z.; Lin, Y.-M.; Rooks, M. J.; Avouris, P. *Physica E* **2007**, *40*, 228 –232.

(4) Li, X.; Wang, X.; Zhang, L.; Lee, S.; Dai, H. *Science* **2008**, *319*, 1229–1232.

(5) Barone, V.; Hod, O.; Scuseria, G. E. *Nano Lett.* **2006**, *6*, 2748–2754.

(6) Son, Y.-W.; Cohen, M. L.; Louie, S. G. *Nature* **2006**, *444*, 347.

(7) Nomura, K.; MacDonald, A. H. *Phys. Rev. Lett.* **2006**, *96*, 256602.

(8) Adam, S.; Hwang, E. H.; Galitski, V. M.; Sarma, S. D. *Proc. Nat. Acad. Sci. U.S.A.* **2007**, *104*, 18392–18397.

(9) Lherbier, A.; Blase, X.; Niquet, Y.-M.; Triozon, F.; Roche, S. *Phys. Rev. Lett.* **2008**, *101*, 036808.

(10) Zhou, S. Y.; Gweon, G.-H.; Fedorov, A. V.; First, P. N.; de Heer, W. A.; Lee, D.-H.; Guinea, F.; Neto, A. H. C.; Lanzara, A. *Nat. Mater.* **2007**, *6*, 770.

(11) Varchon, F.; Feng, R.; Hass, J.; Li, X.; Nguyen, B. N.; Naud, C.; Mallet, P.; Veuillen, J.-Y.; Berger, C.; Conrad, E. H.; Magaud, L. *Phys. Rev. Lett.* **2007**, *99*, 126805.

(12) Emtsev, K. V.; Speck, F.; Seyller, T.; Ley, L.; Riley, J. D. *Phys. Rev. B* **2008**, *77*, 155303.
(13) Kim, S.; Ihm, J.; Choi, H. J.; Son, Y.-W. *Phys. Rev. Lett.* **2008**, *100*, 176802.
(14) Hass, J.; Varchon, F.; Millán-Otoya, J. E.; Sprinkle, M.; Sharma, N.; deer, W. A.; Berger, C.; First, P. N.; Magaud, L.; Conrad, E. H. *Phys. Rev. Lett.* **2008**, *100*, 125504.
(15) Magaud, L.; Hiebel, F.; Varchon, F.; Mallet, P.; Veuillen, J.-Y. *Phys. Rev. B* **2009**, *79*, 161405.
(16) Shemella, P.; Nayak, S. K. *Appl. Phys. Lett.* **2009**, *94*, 032101.
(17) Zhang, Z.; Guo, W. *Appl. Phys. Lett.* **2009**, *95*, 023107.
(18) Chadi, D. J. *Phys. Rev. Lett.* **1979**, *43*, 43–47.
(19) Northrup, J. E. *Phys. Rev. B* **1991**, *44*, 1419.
(20) García, A.; Northrup, J. E. *Phys. Rev. B* **1993**, *48*, 17350.
(21) Rutter, G. M.; Crain, J. N.; Guisinger, N. P.; Li, T.; First, P. N.; Stroscio, J. A. *Science* **2007**, *317*, 219.
(22) Ishigami, M.; Chen, J. H.; Cullen, W. G.; Fuhrer, M. S.; Williams, E. D. *Nano Lett.* **2007**, *7*, 1643.
(23) Albrecht, P. M.; Lyding, J. W. *Appl. Phys. Lett.* **2003**, *83*, 5029–5031.
(24) Ritter, K. A.; Lyding, J. W. *Nat. Mater.* **2009**, *8*, 235.
(25) Albrecht, P. M.; Barraza-Lopez, S.; Lyding, J. W. *Small* **2007**, *3*, 1402–1406.
(26) Lyding, J. W.; Shen, T. C.; Hubacek, J. S.; Tucker, J. R.; Abeln, G. C. *Appl. Phys. Lett.* **1994**, *64*, 2010.
(27) Shen, T. C.; Wang, C.; Abeln, G. C.; Tucker, J. R.; Lyding, J. W.; Avouris, P.; Walkup, R. E. *Science* **1995**, *16*, 1590.
(28) He, K. T.; Koepke, J. C.; Barraza-Lopez, S; Lyding, J. W. *Nano Lett.* **2010**, *10*, 3446.
(29) Rutter, G. M.; Guisinger, N. P.; Crain, J. N.; Jarvis, E. A. A.; Stiles, M. D.; Li, T.; First, P. N.; Stroscio, J. A. *Phys. Rev. B* **2007**, *76*, 235416.
(30) Kohn, W.; Sham, L. J. *Phys. Rev.* **1965**, *140*, A1133–A1138.
(31) Soler, J. M.; Artacho, E.; Gale, J. D.; Garcia, A.; Junquera, J.; Ordejon, P.; Sanchez-Portal, D. *J. Phys.: Condens. Matter* **2002**, *14*, 2745–2779.
(32) Mounet, N.; Marzari, N. *Phys. Rev. B* **2005**, *71*, 205214.
(33) Miwa, R. H.; Orellana, W.; Fazzio, A. *Appl. Phys. Lett.* **2005**, *86*, 213111.
(34) Barraza-Lopez, S.; Albrecht, P. M.; Romero, N. A.; Hess, K. *J. Appl. Phys.* **2006**, *100*, 124304.
(35) Orellana, W.; Miwa, R. H.; Fazzio, A. *Phys. Rev. Lett.* **2003**, *91*, 166802.
(36) Koepke, J. C.; Wood, J. D.; Xu, Y.; Aluru, N. R.; Lyding, J. W. *In 9th IEEE Conference on Nanotechnology* 2009.
(37) Riedl, C; Coletti, C.; Iwasaki, T.; Zakharov, A. A.; Starke, U. *Phys. Rev. Lett.* **2009**, *103*, 246805.